# Lyapunov exponents and extensivity of strongly coupled chaotic maps in regular graphs

Juan Gancio [a], Nicolás Rubido [b,*]

[a] *Universitat Politècnica de Catalunya, Departament de Fisica, Rambla Sant Nebridi 22, Terrassa 08222, Barcelona, Spain*
[b] *University of Aberdeen, King's College, Institute for Complex Systems and Mathematical Biology, AB24 3UE, Aberdeen, United Kingdom*

## A B S T R A C T

In Thermodynamics and Statistical Physics, a system's property is extensive when it grows with the system size. When it happens, the system can be decomposed into separate components, which has been done in many systems with weakly interacting components, such as for various gas models. Similarly, Ruelle conjectured 40 years ago that the Lyapunov exponents (LEs) of some sufficiently large chaotic systems are extensive, which led to study the extensivity properties of chaotic systems with strong interactions. Because of the complexities in these systems, most results achieved so far are restricted to numerical simulations. Here, we derive closed-form expressions for the LEs and entropy rate of coupled maps in finite- and infinite-sized regular graphs, according to the coupling strength, map's chaoticity, and graph's spectral properties. We show that this type of system has either 4 or 5 cases for the LEs, depending on the graph's extreme Laplacian eigenvalues. These cases represent qualitatively different collective behaviours emerging in parameter space, including chaotic synchronisation ($N - 1$ negative LEs) and incoherent chaos ($N$ positive LEs). From the entropy rate, we show that the ring and complete graphs (nearest-neighbour and all-to-all couplings, respectively) are extensive in all parameter regions outside the chaotic synchronisation region. Although our derivations are restricted to one-dimensional maps with constant positive derivative (i.e., chaotic), our approach can be used to find LE and entropy rates for other regular graphs (such as for cyclic graphs) or be the basis for tackling small world graphs via perturbative methods.

## 1. Introduction

Complexity research complements reductionism — it focuses on systems that typically cannot be broken down into smaller subsystems and study separately. The irreducibility in these systems stems from the emergence of collective behaviours that are absent from the isolated subsystems that compose them, due to the strong and non-trivial interaction between these subsystems. These systems are known as complex systems [1–3]. However, for certain complex systems, the collective dynamics can still be simplified to one of barely interacting subsystems. Such behaviour is called *extensive*.

Extensivity is a property used to describe an observable (i.e., of being extensive), such as the energy or entropy of a system. An observable, $Q$, is said to be extensive if it grows with the systems size, $N$ [4] such that $\lim_{N \to \infty} Q/N = $ constant [5]. For example, Clausius' thermodynamic entropy ($H_C = \int \delta q / T$, where $\delta q$ is the heat exchanged between the system and the environment and $T$ the temperature of the system) is proportional to the amount of matter in the system [6] and Boltzmann–Gibbs (BG) entropy ($H_{BG} = -k_B \sum_i p_i \log p_i$, with $k_B$ the

Boltzmann constant and $\{p_i\}$ the probability distribution of accessible micro-states) is proportional to the number of particles in the system (for weakly interacting particles) [7].

For certain chaotic systems, Ruelle conjectured that the system can be decomposed into smaller, identical, and weakly interacting subsystems for system sizes larger than a limit [8]. When this happens, the system's observables can be expressed in terms of these subsystems and the system is extensive. For example, the spectrum of Lyapunov exponents (LE), which quantifies the average exponential divergence or convergence of nearby trajectories, could be expressed as the addition of the identical subsystems' LE spectra. This means that as the system size grows, we can order the system's LE spectrum in decreasing magnitude and plot them using a normalised index (i.e., $i/N \in [0, 1]$) that should converge to a unique curve [9]: the system becomes extensive. This also means the area under the curve for the positive LEs is extensive (i.e., the sum of all the positive LEs), which by Pesin's identity [10] we know is the upper bound to the Kolmogorov–Sinai entropy rate [11]. This property of the LE spectrum – known as Ruelle's

J. Gancio and N. Rubido

*Chaos, Solitons and Fractals: the interdisciplinary journal of Nonlinear Science, and Nonequilibrium and Complex Phenomena 178 (2024) 114392*

conjecture – has been used to determine if chaos in extended systems is extensive [12–18].

Extensive chaos has been studied in various systems, including the Fermi-Pasta–Ulam $\beta$ model [9], the one dimensional Ginzburg–Landau equation [12], Rayleigh–Bénard convection [13,14], the Lorenz-96 model [15], Stuart-Landau oscillators [16,17], and neuronal models [16,18]. However, these studies have focused on numerical simulations, with analytical findings being an oddity; aside some recent results for systems of one-dimensional, chaotic maps of constant derivative, coupled in multiplex networks [19,20].

Here we provide a detailed analytical analysis of the spectrum of LEs for systems of one-dimensional, identical, chaotic maps of constant derivative, coupled diffusively in regular graphs — extending some results from [19,20] and providing novel expressions for LEs and entropy rates. We show that the collective chaotic behaviours determined by the LEs can be classified into 5 cases according to their eigenmodes and the system's control parameters (i.e., coupling strength, individual map's chaoticity, node degree, and graph's Laplacian extreme eigenvalues). We analyse how these 5 cases determine specific regions in parameter space – revealing important information of the underlying attractor – and helping us to derive closed-form expressions for their boundaries, determining critical parameter values. We also derive closed-form expressions for the LEs and entropy rates of the 5 cases when the maps are coupled in a ring or a complete graph (i.e., nearest neighbours and all-to-all couplings, respectively). By analysing the thermodynamic limit of these graphs, we show that the system is extensive in 4 of LE's cases. Extensivity fails only in the parameter region where chaotic synchronisation is achieved, which is the case with $N-1$ negative LEs. We note that this region is vanishingly small for the ring graph but finite in the complete graph.

Our work opens the door to carry similar derivations in coupled systems for the study of extensive chaos. Although our model is restricted to chaotic maps with constant derivative and regular graphs, our results help to improve our understanding of extensive chaos and its limits. For example, our LE classification extends the cases in Refs. [19,20] from 2 to 5. Our derivations of the closed-form expression for the LEs and entropy rates of rings and complete graphs can be used to find the Lyapunov dimension of the emerging attractors by means of the Kaplan-York conjecture [21]. Also, these examples illustrate how our approach can be used to find expressions for other regular graphs, such as for $k$-cycles or $k$-Möbius ladders [22]. Moreover, they can be the basis when changing the graph structure slightly for small-world graphs or multiplex networks, where perturbation theory could be used.

## 2. Model and methods

### 2.1. Spectral properties of regular and cyclic graphs

In this work, we restrict our analysis to coupling chaotic maps in regular graphs. These graphs include the lattices with periodic boundary conditions and random graphs with uniform node degree distribution; namely, any graph where each node has identical number of neighbours. This means that we can define a matrix of node degrees by $\mathbf{K} = k\,\mathbf{I}$ and its inverse by $\mathbf{K}^{-1} = \mathbf{I}/k$, where $k$ is the node degree and $\mathbf{I}$ is the $N \times N$ identity matrix. Hence, the Laplacian matrix is $\mathbf{L} = \mathbf{K} - \mathbf{A} = k\,\mathbf{I} - \mathbf{A}$, with $\mathbf{A}$ being the adjacency matrix ($A_{ij} = 1 = A_{ji}$ if there is a link between nodes $i$ and $j$ or $A_{ij} = 0$ otherwise). In particular, we show results for cyclic graphs, which are a subclass of regular graphs that allows cyclic permutations of nodes and hold a Fourier basis for the eigenvalues and eigenvectors of $\mathbf{L}$ [22–25].

For any graph, Gershgorin's Circle theorem [26] bounds the Laplacian's eigenvalue spectrum to the interval $[0, 2k_M]$, where $k_M$ is the largest node degree. For regular graphs, this implies that $\lambda_n \in [0, 2k]\,\forall n$. Also, regular graphs are connected, implying that there is only one null eigenvalue, $\lambda_0 = 0$ [27], and the rest is bounded between the smallest non-zero eigenvalue $\lambda_F$ – known as the algebraic connectivity or Fiedler

eigenvalue – and the maximum eigenvalue $\lambda_M$. In the infinite limit size, the probability density of eigenvalues in the interval $[\lambda_F, \lambda_M]$ is not null [28–30], which implies dealing with a continuum of eigenvalues for our thermodynamic limit derivations.

### 2.2. Coupled map model

The model we consider here follows the Kaneko model of coupled one-dimensional maps in regular graphs [22,31]. The map iterates are found by

$$\vec{x}_{t+1} = \left[\mathbf{I} - \epsilon\,\mathbf{K}^{-1}\,\mathbf{L}\right]\,\vec{f}(\vec{x}_t), \tag{1}$$

when setting the initial conditions $\{x_0^{(1)}, \dots, x_0^{(N)}\}$, where $0 \le \epsilon \le 1$ is the coupling strength and $\vec{f}(\vec{x}_t) = \{f(x_t^{(1)}), \dots, f(x_t^{(N)})\}$ is a column vector with the $N$ identical mappings of the $t$th iterate states (with $t \in \mathbf{N}$).

### 2.3. Lyapunov exponent and eigenvalue spectra

Lyapunov exponents (LE) measure the average rate of exponential divergence or convergence of orbits close to any particular solution $\{\vec{s}_t\}_{t=0}^{\infty} = \{s_t^{(1)}, \dots, s_t^{(N)}\}_{t=0}^{\infty}$ of Eq. (1). We can find the spectrum of LE of Eq. (1) by considering independent linear perturbations to $\{\vec{s}_t\}_{t=0}^{\infty}$, such that $\vec{x}_t = \vec{s}_t + \vec{\xi}_t$, and by keeping only the leading terms in $\vec{\xi}_t$. This holds

$$\vec{\xi}_{t+1} = \left[\mathbf{I} - \epsilon\mathbf{K}^{-1}\mathbf{L}\right]\mathbf{J}_{\vec{f}}(\vec{s}_t)\,\vec{\xi}_t, \tag{2}$$

where $\mathbf{J}_{\vec{f}}(\vec{s}_t) = \text{diag}\{\partial_1 f(s_t^{(1)}), \dots, \partial_N f(s_t^{(N)})\}$ is the Jacobian matrix of $\vec{f}$ evaluated in the solution $\vec{s}_t$ and $\partial_i f = d\,f/d\,x^{(i)}$ are the derivatives of the mapping components with respect to each independent variable. From Eq. (2) and the Oseledets theorem [32] one can obtain the LE spectrum by taking the time-average of the logarithm of the perturbations. Because the Jacobian depends on $\vec{s}_t$, we would require numerical simulations to find the LEs.

In order to find analytical results, we restrict our analysis to maps with constant derivative $\alpha \in \mathbb{R}$, i.e., $\partial_i f_i(s_t^{(i)}) = \alpha\,\forall i$ and $s_t^{(i)}$. Then, the Jacobian matrix is given by $\mathbf{J}_{\vec{f}}(\vec{s}_t) = \alpha\,\mathbf{I}$ and Eq. (2) can be written as

$$\vec{\xi}_{t+1} = \left[\mathbf{I} - \epsilon\,\mathbf{K}^{-1}\,\mathbf{L}\right]\,\alpha\,\vec{\xi}_t. \tag{3}$$

This is a linear mapping from a constant matrix, $\alpha\left[\mathbf{I} - \epsilon\,\mathbf{K}^{-1}\,\mathbf{L}\right]$, to the perturbations $\vec{\xi}_t$ for each iteration. Moreover, this mapping is valid for any solution $\{\vec{s}_t\}_{t=0}^{\infty} = \{s_t^{(1)}, \dots, s_t^{(N)}\}_{t=0}^{\infty}$ of Eq. (1); including the solution for a synchronous system $s_t^{(1)} = \dots = s_t^{(N)} = s_t\,\forall t$, being $\{\vec{s}_t\}_{t=0}^{\infty} = \{s_t\}_{t=0}^{\infty}\vec{1}$.

We note that for regular graphs, $\mathbf{L}$ can be transformed into a diagonal matrix of real eigenvalues. Namely, $\mathbf{L} = \mathbf{P}\boldsymbol{\Lambda}\mathbf{P}^{-1}$, where $\boldsymbol{\Lambda} = \text{diag}\{\lambda_0, \dots, \lambda_{N-1}\}$ is the eigenvalue spectra and $\mathbf{P} = \{\vec{\psi}_0, \dots, \vec{\psi}_{N-1}\}$ is the matrix containing the (column) eigenvectors, such that $\mathbf{L}\,\vec{\psi}_n = \lambda_n\,\vec{\psi}_n\,\forall n$. Consequently, we can change variables in Eq. (3) to $\vec{\zeta}_t = \mathbf{P}^{-1}\vec{\xi}_t$, and the perturbations to $\{\vec{s}_t\}_{t=0}^{\infty}$ become decoupled in the $N$ eigenmodes ($n = 0, 1, \dots, N-1$) according to

$$\zeta_{t+1}^{(n)} = \left(1 - \epsilon\,\lambda_n/k\right)\alpha\,\zeta_t^{(n)}, \tag{4}$$

where the solution $\zeta_t^{(n)} = e^{\chi_n t}\zeta_0^{(n)}$ gives the LE spectrum, $\{\chi_n\}_{n=0}^{N-1}$ [33–35],

$$\chi_n = \log\left|1 - \epsilon\,\frac{\lambda_n}{k}\right| + \alpha = \chi_{top}\left(\epsilon\lambda_n/k\right) + \chi_{dyn}. \tag{5}$$

$\chi_{dyn} = \alpha$ is the contribution to $\chi_n$ from the one-dimensional mapping dynamics and $\chi_{top}$ is the contribution from the topology. We note that the zeroth mode is $\chi_0 = \chi_{dyn} = \alpha$ because $\lambda_0 = 0$ (always). Also, $\lambda_n \in [0, 2k]$, then $\chi_{top}(\epsilon\lambda_n/k) < 0\,\forall n > 0$. In this work, we focus on chaotic maps, $\chi_{dyn} > 0$, so that the LE spectrum can have positive values (i.e., when $\chi_{top} + \chi_{dyn} > 0$).

J. Gancio and N. Rubido

*Chaos, Solitons and Fractals: the interdisciplinary journal of Nonlinear Science, and Nonequilibrium and Complex Phenomena 178 (2024) 114392*

## 2.4. Entropy rate, specific entropy rate, and extensivity

The LE are related to other invariant measures of a dynamical system. For example, the entropy rate – or Kolmogorov–Sinai entropy – is the production of entropy per unit of time and has an upper bound $h$ given by the sum of positive LE. This relationship is known as the Pesin identity [10],

$$h = \sum_{n \in \mathcal{P}} \chi_n, \quad \text{where } \mathcal{P} = \{n \in [0, N-1] \subset \mathbb{N} : \ \chi_n > 0\}. \tag{6}$$

In this work, we find closed-form expressions for $h$ and study its dependency with the system size, particularly, in the thermodynamic limit ($N \to \infty$). The reason behind this study is assessing the extensivity of our coupled maps. An observable $Q(x^{(1)}, \ldots, x^{(N)})$ is said to be extensive if it scales proportionally with $N$ [4] such that $\lim_{N \to \infty} Q(x^{(1)}, \ldots, x^{(N)})/N = \text{constant}$ [4,5]. Thus, we define a specific entropy rate, $\eta = h/N$, and refer to our coupled maps as extensive if $\lim_{N \to \infty} \eta = \text{constant}$.

## 3. Results

Here, we introduce a classification for the spectrum of Lyapunov exponents (LEs) of qualitatively different dynamical scenarios emerging in a system of chaotic maps with constant derivative coupled in generic regular graphs. Our classification depends on the sign of the LEs, where the resultant dynamical scenarios include: only having chaotically divergent directions with positive LEs, having a mix of divergent and convergent directions with positive and negative LEs, or having one positive LE and then convergent directions with negative LEs, which is the regime of chaotic synchronisation. Moreover, we distinguish 3 types of scenarios for the case of mixed LE signs with different emerging properties.

Our classification is constructed by analysing the coupling strength $\epsilon$, maps' chaoticity $\chi_{dyn}$, and topological characteristics of the graph, including the node degree $k$, Laplacian eigenvalue properties, and system size $N$. Our results include closed-form expressions and illustrations in parameter space of the classification boundaries and critical control parameters as well as particular derivations for the ring and complete graph (all-to-all coupling). Importantly, we show how our classification and closed-form expressions help to determine the entropy rate and extensive properties for these particular graphs, fulfilling Ruelle's conjecture outside the synchronous region.

### 3.1. General classification of Lyapunov exponents' spectra according to control parameters and graph's characteristics

According to Eq. (5), the system's LEs are a function of the map's chaoticity, $\chi_{dyn}$, coupling strength, $\epsilon$, and the normalised Laplacian eigenvalues of the graph, $\lambda_n/k$, which depend implicitly on the system size, $N$. We note that the absolute value in Eq. (5) creates a folding in the LE spectrum when $\epsilon \lambda_n/k > 1$. This means that, even if the eigenvalues of the Laplacian matrix $\mathbf{L}$ are ordered such that $\lambda_0 = 0 < \lambda_1 \leq \cdots \leq \lambda_{N-1}$, the LEs are not ordered according to the eigenvalues. In what follows, we use this folding to introduce our LE classification and derive the limits of validity in each class.

We distinguish 3 cases for the LE spectrum, which are illustrated by vertical continuous lines in Fig. 1. For finite regular graphs, these lines are discrete sets of points, whose distribution depends on the graph's topological properties. The parameter region that generates negative LEs is highlighted by the horizontal (middle) blue shaded area (with well-defined bounds). Positive LEs are generated outside of it, within the pink shaded areas.

We refer to *Case 1 when all LEs are positive*, $\{\chi_n\}_{n=0}^{N-1} > 0$ (leftmost vertical line in Fig. 1); namely, $\chi_{top} + \chi_{dyn} > 0$, $\forall n$ in Eq. (5). This case implies chaotic collective dynamics and happens only if there are no folded modes in Eq. (5). Initially, we can get Case 1 either by having

$0 < \epsilon \lambda_n/k < 1 - \exp(-\chi_{dyn})$, $\forall n > 0$ (when $1 - \epsilon \lambda_n/k > 0$) or by having $1 + \exp(-\chi_{dyn}) < \epsilon \lambda_n/k < 2$, $\forall n > 0$ (when $1 - \epsilon \lambda_n/k < 0$). However, the second condition, which corresponds to having only folded modes, cannot happen in any regular graph except for the complete graph, where $\lambda_n/k = N/N - 1$, $\forall n > 0$ [27].

In opposition, we refer to *Case 3 when all LEs are negative* – with the exception of the first mode, $n = 0$, which is always positive (rightmost vertical line in Fig. 1). Namely, $\chi_{top} + \chi_{dyn} < 0$ $\forall n > 0$ or equivalently $\{\chi_n\}_{n=1}^{N-1} < 0$. This case corresponds to having a completely synchronous chaos, and happens only if $1 - \exp(-\chi_{dyn}) < \epsilon \lambda_n/k < 1 + \exp(-\chi_{dyn})$, $\forall n > 0$ [22].

In between these cases, we refer to *Case 2 when the system can have positive and negative LEs* (and null LEs). There are 3 possibilities to obtain mixed signs in the LE spectrum, which we introduce as Types I, II, and III and represent by 3 central vertical lines in Fig. 1. Case 2 - Type I happens when the positive part of the LE spectrum is obtained from unfolded modes, i.e., for $n$, $\epsilon$, and $k$, such that $0 < \epsilon \lambda_n/k < 1$, which implies $0 < 1 - \epsilon \lambda_n/k$ in Eq. (5). Case 2 - Type II happens when the positive LEs are obtained from folded modes, which implies $1 - \epsilon \lambda_n/k < 0$ in Eq. (5) for those modes. Case 2 - Type III has positive LEs from both folded and unfolded modes.

We note that the position and existence of the different cases in parameter space is mainly dependent on the value of $\lambda_F$, $\lambda_M$, and $k$, which are topological characteristics. The normalised Fiedler eigenvalue, $\lambda_F/k$, determines the lower end of any vertical segment in Fig. 1, and the normalised maximum eigenvalue, $\lambda_M/k$, determines the upper end of any vertical segment in Fig. 1. Namely, $\lambda_F/k$ and $\lambda_M/k$ bound the LE spectrum. In the case of a complete (all-to-all) graph, $\lambda_F/k = \lambda_M/k = N/(N-1) = \lambda_n/k$, which means that instead of vertical lines in Fig. 1 there is a single point. Consequently, the LEs of an all-to-all coupled map system either fall under Case 1 or 3.

### 3.2. Universal parameter regions and explicit boundaries for our classification of Lyapunov spectra

The lines that separate the different shaded areas in Fig. 1 correspond to null LEs, i.e., when $\chi_{top}(\epsilon \lambda_n/k) + \chi_{dyn} = 0$ in Eq. (5) for some $n > 0$, which imply that $\epsilon \lambda_n/k = 1 \pm \exp(-\chi_{dyn})$ for that $n$. The limits for the different LE cases appear when either $n = F$ or $M$, since then, the remaining modes hold either larger ($\lambda_n/k \geq \lambda_F/k$) or smaller ($\lambda_n/k \leq \lambda_M/k$) values. This allows us to analyse the critical values that the other control parameters take – namely, $\epsilon$ and $\chi_{dyn}$ – when following the null LE condition, deriving closed-form expressions for the limits of the 3 LE cases in the ($\epsilon$, $\chi_{dyn}$) parameter space. These results are represented in Fig. 2, where we differentiate the LE spectrum cases and types according to whether the regular graph is such that $\lambda_F + \lambda_M > 2k$ or such that $\lambda_F + \lambda_M < 2k$. We discuss the reason behind this topological differentiation in Case 3 and 2, but we have also reported it emerging in the context of coupled-maps' synchronisation [22].

For a finite $\chi_{dyn}$ and sufficiently small $\epsilon$, the LE spectrum falls in the Case 1 category — namely, $\chi_n > 0$ $\forall n$. It remains as a Case 1 until $\chi_{dyn}$ is decreased or $\epsilon$ increased enough to have $\epsilon \lambda_M/k = 1 - \exp(-\chi_{dyn})$, which is represented by the lowest horizontal dashed line in Fig. 1. After that point, negative LEs appear and we leave Case 1 — the completely incoherent chaotic regime ends. This implies that the boundary of Case 1 is

$$\epsilon^{(1)} \frac{\lambda_M}{k} = 1 - \exp(-\chi_{dyn}) \ \Rightarrow \ \epsilon^{(1)} = \left[1 - \exp(-\chi_{dyn})\right] \left(\frac{\lambda_M}{k}\right)^{-1}, \tag{7}$$

which defines a critical $\epsilon$ as a function of $\chi_{dyn}$ – inverting Eq. (7) holds the minimal $\chi_{dyn}$ as a function of $\epsilon$. So, given a $\chi_{dyn} > 0$ and while $\epsilon < \epsilon^{(1)}$, the system is in a completely incoherent chaotic regime with a LE spectrum in Case 1, which corresponds to the ($\epsilon$, $\chi_{dyn}$) parameter regions on the left of the panels in Fig. 2 (blue shaded areas).

On the other hand, for a finite $\epsilon$ and sufficiently small (but positive) $\chi_{dyn}$, the LE spectrum falls in the Case 3 category — namely, $\chi_n < $

J. Gancio and N. Rubido

Chaos, Solitons and Fractals: the interdisciplinary journal of Nonlinear Science, and Nonequilibrium and Complex Phenomena 178 (2024) 114392
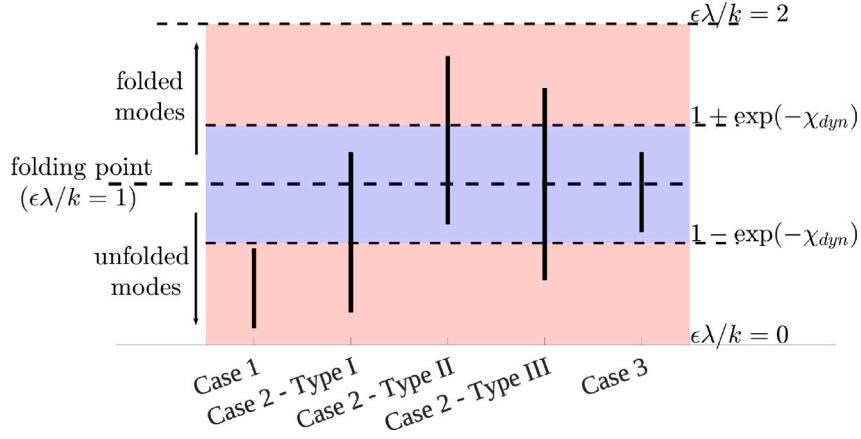


**Fig. 1.** Classification of Lyapunov exponents of coupled maps according to control parameters and graph characteristics. Vertical lines represent the normalised non-zero eigenvalues of a generic regular graph, $\lambda_n/k$ ($n = 1, \ldots, N-1$ the eigenmodes), multiplied by the coupling strength $\epsilon$ between identical chaotic maps ($\epsilon \in [0, 1]$), i.e., $\epsilon \lambda_n/k$. The resultant Lyapunov exponents (LEs) depend on the map's (isolated and fixed) chaoticity, $\chi_{dyn}$, and $\epsilon \lambda/k$ [see Eq. (5)], creating different cases for the LEs' signs. Negative [Positive] LEs fall within [outside] the centrally shaded blue region.
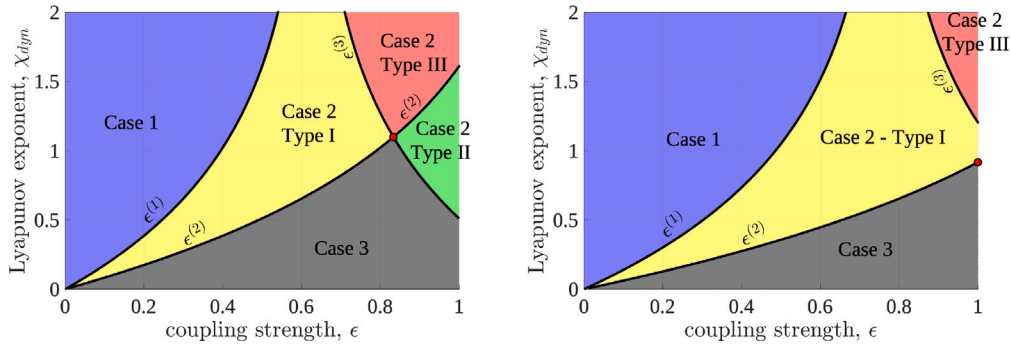


**Fig. 2.** Analytic representation of the different cases of Lyapunov spectra in parameter space for chaotic maps coupled in generic regular graphs. Left [Right] panel: 5 different cases of Lyapunov exponents [as in Fig. 1] emerging from the coupled system when the graph's Laplacian eigenvalues are such that $\lambda_F + \lambda_M > 2k$ [$\lambda_F + \lambda_M < 2k$], $\lambda_F$ and $\lambda_M$ being the Fiedler and largest Laplacian eigenvalues, respectively. Cases are represented with different coloured regions, whose boundaries are determined by the critical coupling strength curves $\epsilon^{(1)}$ [Eq. (7)], $\epsilon^{(2)}$ [Eq. (8)], and $\epsilon^{(3)}$ [Eq. (9)].

$0 \; \forall n > 0$. It remains as a Case 3 until $\chi_{dyn}$ is increased enough or $\epsilon$ is either decreased until $\epsilon \lambda_F/k = 1 - \exp(-\chi_{dyn})$ (which corresponds to having the smallest mode reach the lowest horizontal dashed line in Fig. 1) or increased until $\epsilon \lambda_M/k = 1 + \exp(-\chi_{dyn})$ (which corresponds to having the largest mode reach the highest horizontal dashed line in Fig. 1). Crossing these limits creates a positive LE and we leave Case 3 – the completely synchronous chaotic regime ends. So, the lower bound of Case 3 is

$$\epsilon^{(2)} = \left[1 - \exp(-\chi_{dyn})\right] \left(\frac{\lambda_F}{k}\right)^{-1}, \qquad (8)$$

and the upper bound of Case 3 is

$$\epsilon^{(3)} = \left[1 + \exp(-\chi_{dyn})\right] \left(\frac{\lambda_M}{k}\right)^{-1}, \qquad (9)$$

which define a critical $\epsilon$ as a function of $\chi_{dyn}$ – inverting Eq. (8) or (9) gives a maximal $\chi_{dyn}$. When $\epsilon = \epsilon^{(2)}$ or $\epsilon = \epsilon^{(3)}$, a LE becomes null, but when the graph is such that $\lambda_F + \lambda_M < 2k$, $\epsilon^{(3)}$ cannot be reached for any $\epsilon \in (0, 1]$ for such a small $\chi_{dyn}$. Overall, the ($\epsilon$, $\chi_{dyn}$) parameter regions where Case 3 is valid are located on the bottom of the panels in Fig. 2 (grey shaded areas).

The intersection of the critical $\epsilon^{(2)}$ line with $\epsilon^{(3)}$ or $\epsilon = 1$ determines the maximum chaoticity that can be synchronised, $\chi_{dyn}^{max}$, in regular graphs with $\lambda_F + \lambda_M > 2k$ or $\lambda_F + \lambda_M < 2k$, respectively. $\chi_{dyn}^{max}$ is signalled by a filled circle in Fig. 2 and has the following expressions

for the respective graphs

$$\begin{cases} \chi_{dyn}^{max} = -\log\left[\frac{1-(\lambda_F/\lambda_M)}{1+(\lambda_F/\lambda_M)}\right] = 2\tanh^{-1}\left(\frac{\lambda_F}{\lambda_M}\right), \\ \chi_{dyn}^{max} = -\log\left[1 - \frac{\lambda_F}{k}\right], \end{cases} \qquad (10)$$

which are derived from making $\epsilon^{(2)} = \epsilon^{(3)}$ and $\epsilon^{(2)} = 1$, respectively. These maximal values determine whether $\chi_{dyn}$ is sufficiently small or not (see [22]).

In between Cases 1 and 3, the LE spectra falls in the Case 2 category — namely, the system can have positive, null, and negative LEs, with collective dynamics that can include synchronous clusters or chimera states. The three types of Case 2 are represented in the ($\epsilon$, $\chi_{dyn}$) parameter regions of Fig. 2 by the yellow (Case 2 - Type I), red (Case 2 - Type III), and green (Case 2 - Type II) shaded areas, where the latter appears only if the graph is such that $\lambda_F + \lambda_M > 2k$ (left panel of Fig. 2).

Case 2 - Type I happens when $\epsilon^{(1)} < \epsilon < \min\{\epsilon^{(2)}, \epsilon^{(3)}, 1\}$, where the positive part of the LE spectrum comes from unfolded modes, i.e., $0 < \epsilon \lambda_n/k < 1$ for those $n$ (see Fig. 1). A Case 2 - Type I happens when we increase $\epsilon$ from Case 1 (i.e., $\epsilon > \epsilon^{(1)}$) or as we decrease $\epsilon$ from Case 3 – as long as the regular graph is not a complete graph. This means that the lower bound of Case 2 - Type I is $\epsilon^{(1)}$, but the upper bound depends on the value of $\chi_{dyn}$ (which happens when $\epsilon \lambda_M/k = 1 + \exp(-\chi_{dyn})$) and on the graph being such that $\lambda_F + \lambda_M > 2k$ or $< 2k$. For $\chi_{dyn} > \chi_{dyn}^{max}$ [Eq. (10)], the upper bound of Case 2 - Type I is $\min\{\epsilon^{(3)}, 1\}$. For

J. Gancio and N. Rubido

*Chaos, Solitons and Fractals: the interdisciplinary journal of Nonlinear Science, and Nonequilibrium and Complex Phenomena 178 (2024) 114392*

$\chi_{dyn} < \chi_{dyn}^{max}$ [Eq. (10)], the upper bound of Case 2 - Type I is $\epsilon^{(2)}$. These bounds, i.e., $\epsilon^{(1)} < \epsilon < \min\{\epsilon^{(2)}, \epsilon^{(3)}, 1\}$, define the yellow shaded area in Fig. 2 for the regular graphs fulfilling $\lambda_F + \lambda_M > 2k$ (left panel) and $\lambda_F + \lambda_M < 2k$ (right panel).

Case 2 - Type II happens when the positive part of the LE spectrum comes from folded modes (in opposition to Case 2 - Type I). This implies that $\epsilon \lambda_n/k > 1$ in Eq. (5) for those modes (see Fig. 1), which can only happen in regular graphs fulfilling $\lambda_F + \lambda_M > 2k$. The upper bound of Case 2 - Type II is $\epsilon = 1$, but the lower bound depends on whether $\chi_{dyn} < \chi_{dyn}^{max}$ or $\chi_{dyn} > \chi_{dyn}^{max}$ [Eq. (10)]. If $\chi_{dyn} < \chi_{dyn}^{max}$, then the lower bound is $\epsilon^{(3)} < \epsilon \leq 1$. If $\chi_{dyn} > \chi_{dyn}^{max}$, then the lower bound is $\epsilon^{(2)} < \epsilon \leq 1$. When $\chi_{dyn} = \chi_{dyn}^{max}$, $\epsilon^{(2)} = \epsilon^{(3)}$. Consequently, Case 2 - Type II only appears on the left panel of Fig. 2 as a green shaded area.

Case 2 – Type III has positive LEs from folded and unfolded modes and con only occur if $\chi_{dyn} > \chi_{dyn}^{max}$ [Eq. (10)]. It is bounded by Case 2 - Type I and Case 2 - Type II. Thus, the parameter region of Case 2 – Type III is $\epsilon^{(3)} < \epsilon < \min\{\epsilon^{(2)}, 1\}$, which is represented as red shaded areas in Fig. 2.

### 3.3. Application of our Lyapunov spectra classification in an extensivity analysis of coupled maps in ring graphs

Now we show how our classification differentiates the emerging dynamics for a set of coupled chaotic maps in ring graphs ($C_N(k)$ where $k = 2$) of different sizes. We study the emerging dynamics according to $\epsilon$ and $\chi_{dyn}$, quantifying the complexity of the underlying attractors in this parameter space with the entropy rate $h$ [Eq. (6)] and showing which dynamics are extensive in the thermodynamic limit (i.e., $\lim_{N\to\infty} h/N \to$ constant).

For $C_N(2)$, the Laplacian eigenvalues are $\lambda_n[C_N(2)] = 2[1 - \cos(2\pi n/N)] = 4\sin^2(\pi n/N)$ with $n = 0, \ldots, N-1$ [22,25,27]. Thus, they contain degeneracies (i.e., most eigenvalues have multiplicity $= 2$), with the exception of $\lambda_0 = 0$ and, if $N$ is odd, the maximum eigenvalue $\lambda_M$. So, we can sort them: $\lambda_0 = 0 < \lambda_1 = \lambda_F = \lambda_{N-1} \leq \lambda_2 = \lambda_{N-2} \leq \lambda_3 = \lambda_{N-3} \leq \cdots \leq \lambda_{\lfloor N/2 \rfloor} = \lambda_M$, which is relevant when separating folded from unfolded LE modes. In particular, the LEs of coupled maps $\chi_n$ [Eq. (5)] in $C_N(2)$ are given by

$$\chi_n[C_N(2)] = \log\left|1 - 2\epsilon \sin^2\left(\frac{\pi n}{N}\right)\right| + \chi_{dyn}, \text{ with } n = 0, \ldots, N-1. \quad (11)$$

We note that $\lambda_F[C_N(2)] = 4\sin^2(\pi/N)$ and $\lambda_M[C_N(2)] = 4\sin^2(\pi/2) = 4$, which means that $\lambda_F + \lambda_M > 2k = 4$ and Case 2 - Type II can be achieved (see left panel in Fig. 2). With $\lambda_F$ and $\lambda_M$ we derive the following equations for the boundaries of our LE classification [Eqs. (7), (8), and (9)]:

$$\epsilon^{(1)}_{C_N(2)} = \frac{1 - e^{-\chi_{dyn}}}{2}, \quad \epsilon^{(2)}_{C_N(2)} = \frac{1 - e^{-\chi_{dyn}}}{2\sin^2(\pi/N)}, \quad \epsilon^{(3)}_{C_N(2)} = \frac{1 + e^{-\chi_{dyn}}}{2}, \quad (12)$$

which for $\chi_{dyn} \to \infty$ tend to $\epsilon^{(1)}_{C_N(2)}(\chi_{dyn} \to \infty) = \epsilon^{(3)}_{C_N(2)}(\chi_{dyn} \to \infty) = 1/2$ independently of $N$, and $\epsilon^{(2)}_{C_N(2)}(\chi_{dyn} \to \infty) = 1/2\sin^2(\pi/N)$.

*Extensivity in ring graphs.* To analyse whether the emerging dynamics from coupled maps in $C_N(2)$ is extensive, we analyse the Thermodynamic limit of the specific entropy $\eta = h/N$ by using Eq. (11) – $\eta$ should tend to a constant when $N \to \infty$ if the system is extensive. In what follows, we assume $\chi_{dyn}$ constant (for simplicity) and treat $\eta$ as a function of $\epsilon$ and $N$: $\eta = \eta(\epsilon, N)$.

For the parameter region where the LEs fall under our Case 1 classification (namely, when all LEs are positive), the entropy rate in $C_N(2)$ graphs is

$$h_1 = N\chi_{dyn} + \sum_{n=1}^{N-1} \log\left[1 - 2\epsilon \sin^2\left(\frac{\pi n}{N}\right)\right] > 0. \quad (13)$$

To get an expression of $h$ as a function of $N$, we expand the logarithm in a Maclaurin series, $h_1 = N\chi_{dyn} - \sum_{k=1}^{N-1}\left[\sum_{j=1}^{\infty}\left[2\epsilon \sin^2\left(\frac{\pi k}{N}\right)\right]^j \frac{1}{j}\right]$,

and note that the first three terms are closed sums (See Appendix: Closed sums derivation). This allows us to express Eq. (13) as $h_1 = N\chi_{dyn} - \epsilon N - \frac{3}{4}\epsilon^2 N - \frac{5}{6}\epsilon^3 N + \mathcal{O}(\epsilon^4)$, which is positive by construction (in spite of the negative terms). Consequently, we can say that in the chaotically incoherent region of Case 1 and up to fourth order in $\epsilon$, $\eta_1(\epsilon, N) = h_1/N \simeq \chi_{dyn} - \epsilon - \frac{3}{4}\epsilon^2 - \frac{5}{6}\epsilon^3$ is constant and the system is extensive when $\epsilon$ is kept constant and $N \to \infty$.

For the Case 2 - Type I region, the positive part of the LE spectrum is obtained from unfolded modes (see Fig. 1), and these are the only modes included in $h$ when doing the summation of Eq. (6). This means that the positive LEs come from the first Laplacian eigenvalues up to mode $P(\epsilon, \chi_{dyn}, N)/2$ and their corresponding degenerate modes. Namely, from the set of eigenvalues $\{\lambda_0, \lambda_1, \lambda_{N-1}, \lambda_2, \lambda_{N-2}, \ldots, \lambda_{\frac{P}{2}}, \lambda_{N-\frac{P}{2}}\}$.

To determine $P(\epsilon, \chi_{dyn}, N)$, we find the LE mode $n = P(\epsilon, \chi_{dyn}, N)/2$ such that $\chi_n[C_N(2)] = 0$. We do this by inverting Eq. (11), which holds

$$P(\epsilon, \chi_{dyn}, N) = \left\lfloor \frac{N}{\pi} \arcsin\left[\sqrt{\frac{1 - \exp(-\chi_{dyn})}{2\epsilon}}\right]\right\rfloor < N - 1, \quad (14)$$

where $\lfloor \cdot \rfloor$ is the floor operator, rounding the argument to the closest lower integer. We note from Eq. (14) that $P \propto N$ and we can use it to define the entropy rate of Case 2 - Type I, $h_{2,I}$, by

$$h_{2,I} = (P + 1)\chi_{dyn} + 2\sum_{n=1}^{P/2} \log\left[1 - 2\epsilon \sin^2\left(\frac{\pi n}{N}\right)\right], \quad (15)$$

where the multiplicative factor 2 comes from the multiplicity (degeneracy) of these eigenmodes. In the limit $N \to \infty$, the summation in Eq. (15) can be replaced by an integral. Thus, $h_{2,I} = (P + 1)\chi_{dyn} + 2\frac{N}{\pi}\int_0^{x_{max}} \log\left|1 - 2\epsilon \sin^2(x)\right| dx$, with $x_{max} = \frac{\pi}{N}\frac{P}{2}$, which is independent of $N$. Consequently, we have that $h_{2,I} \propto N$ when $N \to \infty$, making the system extensive in this dynamical region as well.

For the Case 2 - Type III region, there are positive LEs coming from folded and unfolded modes. The number of unfolded modes is found as in Case 2 - Type I; meaning that there are $P_1$ unfolded modes given by Eq. (14). Then, there are $P_2$ folded modes given by

$$P_2 = (N - 1) - \left\lfloor \frac{N}{\pi} \arcsin\left[\sqrt{\frac{1 + \exp(-\chi_{dyn})}{2\epsilon}}\right]\right\rfloor < N - 1, \quad (16)$$

which we find by inverting Eq. (11) when the argument of the absolute value is negative. This means that in total, there are $P = P_1 + P_2 + 1$ positive LEs in this case (where the +1 comes from the null Laplacian eigenvalue). Thus, the entropy rate for Case 2 - Type III is

$$h_{2,III} = (P_1 + P_2 + 1)\chi_{dyn} + 2\sum_{n=1}^{P_1/2} \log\left[1 - 2\epsilon \sin^2\left(\frac{\pi n}{N}\right)\right]$$
$$+ 2\sum_{n=P_2/2}^{N/2} \log\left[2\epsilon \sin^2\left(\frac{\pi n}{N}\right) - 1\right], \quad (17)$$

where $P_1$ is determined by Eq. (14) and $P_2$ by Eq. (16). We note also that both numbers are proportional to $N$.

In the thermodynamic limit, $N \to \infty$, we can replace the summations in Eq. (17) by integrals. This holds $h_{2,III} = (P_1 + P_2 + 1)\chi_{dyn} + 2\frac{N}{\pi}\int_0^{x_{max}} \log[1 - 2\epsilon \sin^2(x)] dx + 2\frac{N}{\pi}\int_{x_{min}}^{\pi/2} \log[2\epsilon \sin^2(x) - 1] dx$, with $x_{max} = \frac{\pi}{N}\frac{P_1}{2}$ and $x_{min} = \frac{\pi}{N}\frac{P_2}{2}$, making them independent of the system size. Consequently, we have that $h_{2,III} \propto N$ when $N \to \infty$, making this type of chaos extensive.

Similarly, we can find an expression for the entropy rate of Case 2 - Type II, which corresponds to having positive LEs coming solely from folded modes. This means that the number of folded modes is given by Eq. (16), making the resultant entropy rate extensive; as in the previous cases. Overall, Case 1 and Case 2 are all extensive for the ring graph, with the exception being Case 3, where the system is completely synchronous.
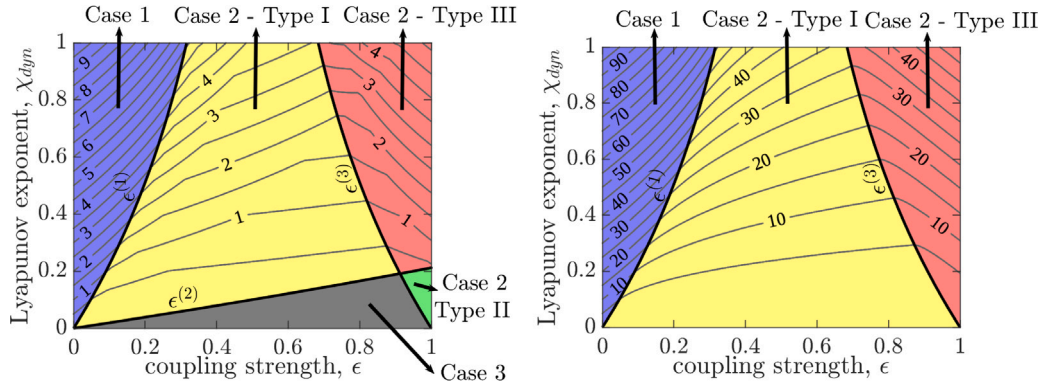
**Fig. 3.** Regions with different Lyapunov spectra and entropy rates for coupled maps in ring graphs. Control parameters: coupling strength between maps, $\epsilon$, and map's chaoticity before coupling, $\chi_{dyn}$. Left panel: 5 regions with different collective dynamics for $N = 10$ chaotic maps according to the coupled system's Lyapunov exponents (coloured areas), where boundaries are the critical coupling strengths $\epsilon^{(1)}$, $\epsilon^{(2)}$, and $\epsilon^{(3)}$ [Eq. (12)]. Contour lines show constant-valued entropy rates, $h$, crossing the parameter space [Eqs. (13), (15), and (17)]. Right panel: same results but for $N = 100$ maps.
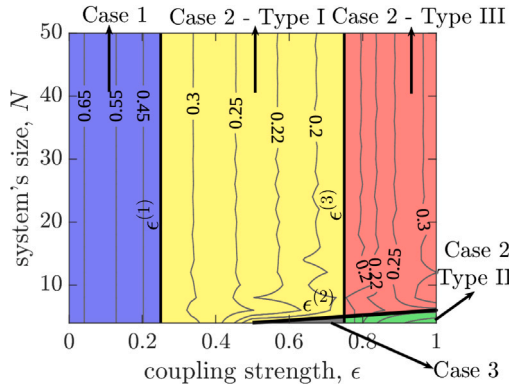


**Fig. 4.** Specific entropy rates for chaotic maps coupled in ring graphs. The chaotic maps have fixed chaoticity of $\chi_{dyn} = \log(2)$ when isolated and their coupled dynamics is controlled by the coupling strength $\epsilon$ and system size $N$ changes. Shaded regions differentiate our 5 Lyapunov exponent cases from the maps' emerging dynamics – as in Figs. 2 and 3 with the same colour scheme – and are separated by the boundaries $\epsilon^{(1)}$, $\epsilon^{(2)}$, and $\epsilon^{(3)}$ [Eq. (12)]. Contour lines show constant values for the specific entropy rate, $\eta = h/N$, in the different cases [Eqs. (13), (15), and (17)].

*Examples for finite ring graphs.* As an example, here we relate the values of $h$ from Eqs. (13), (15), and (17) for two ring graphs with $N = 10$ and 100 maps in the $(\epsilon, \chi_{dyn})$ parameter space with their emerging dynamics. The values of $h$ are shown in Fig. 3 as contour lines, with coloured regions indicating the location of the cases from our LE classification.

We can see from Fig. 3 that the different emerging dynamics – corresponding to the different cases in our LE classification – influence directly the resultant entropy rate of the system. This is expected, since each parameter region corresponds to a different collective dynamic.

For example, Case 3 in the left panel of Fig. 3 corresponds to the emergence of synchronous chaotic states. This implies that the only mode contributing to the Pesin identity [Eq. (6)] for this dynamics is the null eigenmode ($\mathcal{P} = \{n = 0\}$), resulting in $h_3 = \chi_{dyn}$ and making the system non-extensive. Within this parameter region, entropy rate constant values correspond to horizontal lines, which means that increasing $\epsilon$ keeps $h$ constant (as long as $\chi_{dyn}$ is fixed). However, as the system size is increased, this region almost vanishes, as in the right panel of Fig. 3. In fact, for sufficiently small $\chi_{dyn}$ (i.e., $\chi_{dyn} < -\log|1 - \epsilon\,\lambda_F/2| = -\log|1 - \epsilon\,2\sin^2(\pi/N)|$) the finite-sized system can synchronise ($-\log|1 - \epsilon\,2\sin^2(\pi/N)| \to 0$ as $N \to \infty$).

From the entropy rate contour lines in Fig. 3, we can see that changing the control parameters – $\epsilon$ or $\chi_{dyn}$ – can have different effects on the value of $h$. For example, increasing $\epsilon$ at constant $\chi_{dyn}$ in the

regions of Case 1 (blue area) and Case 2 - Type I (yellow area) decreases $h$. This means that the chaotic attractor in these parameter regions becomes less complex for increasing $\epsilon$. On the other hand, increasing $\epsilon$ at constant $\chi_{dyn}$ in the region of Case 2 - Type II (green area) and III (red areas) increases $h$. This means that the chaotic attractor in this parameter region becomes more complex for increasing $\epsilon$, which is somewhat counter-intuitive (but stems from the folding of modes).

In order to illustrate how Eqs. (13), (15), and (17) determine the changes in $h$ for a ring graph as $N$ is increased, we shown in Fig. 4 the constant values of $\eta = h/N$ (in contour lines) for maps with $\chi_{dyn} = \log(2)$. In this case, the dynamical regions are divided by the critical coupling strengths from Eq. (12): $\epsilon^{(1)}_{C_N(2)} = 1/4$, $\epsilon^{(2)}_{C_N(2)} = 1/4\sin^2(\pi/N)$, and $\epsilon^{(3)}_{C_N(2)} = 3/4$. We can see that the specific entropy rate $\eta$ tends to become a straight vertical line for any $\epsilon$ as $N$ is increased, meaning that the system becomes extensive.

For $\chi_{dyn} = \log(2)$, it has already been shown that the synchronous solution is always unstable if $N > 5$ [35], even more, $\lambda_F(N = 6) = 1$, which implies that that the curve $\epsilon^{(2)}(N = 6) = 1$ (see Fig. 4). Thus, for $\chi_{dyn} = \log(2)$ and $N > 6$, only Case 1, Case 2 – Type I, and Case 2 – Type III exist.

*Application of our Lyapunov spectra classification in an extensivity analysis of coupled maps in complete graphs*

Here we show how our classification differentiates the emerging dynamics for a set of coupled chaotic maps in complete graphs ($C_N(k)$, where $k = N - 1$) of different sizes. We study the emerging dynamics as a function of $\epsilon$ and $\chi_{dyn}$, quantifying the complexity of the underlying attractors by the entropy rate $h$ [Eq. (6)] and showing which dynamics are extensive in the thermodynamic limit (i.e., $\lim_{N\to\infty} h/N \to$ constant).

For $C_N(N - 1)$, the non-zero Laplacian eigenvalues are identical, i.e., $\lambda_n[C_N(N - 1)] = N$ with $n = 1, \dots, N - 1$ [22,25,27]. Thus, the LEs $\chi_n$ [Eq. (5)] in $C_N(N - 1)$ are also identical,

$$\chi_n[C_N(N - 1)] = \log\left|1 - \epsilon\,\frac{N}{N - 1}\right| + \chi_{dyn}, \text{ with } n = 1, \dots, N - 1, \quad (18)$$

with $\chi_0[C_N(N - 1)] = \chi_{dyn}$. Moreover, $\lambda_F = \lambda_M = N$, such that $\lambda_F + \lambda_M > 2k = 2(N - 1)$, which again implies that Case 2 - Type II can be achieved (see Fig. 2). However, because of this multiplicity in the Laplacian eigenvalues, the critical coupling strengths bounding Case 2 - Type I and Type III blend, making these cases disappear. Namely, from Eqs. (7), (8), and (9), we get

$$\epsilon^{(1)}_{C_N(N-1)} = \left(1 - e^{-\chi_{dyn}}\right)\frac{(N - 1)}{N} = \epsilon^{(2)}_{C_N(N-1)},$$

$$\epsilon^{(3)}_{C_N(N-1)} = \left(1 + e^{-\chi_{dyn}}\right)\frac{(N - 1)}{N}. \quad (19)$$
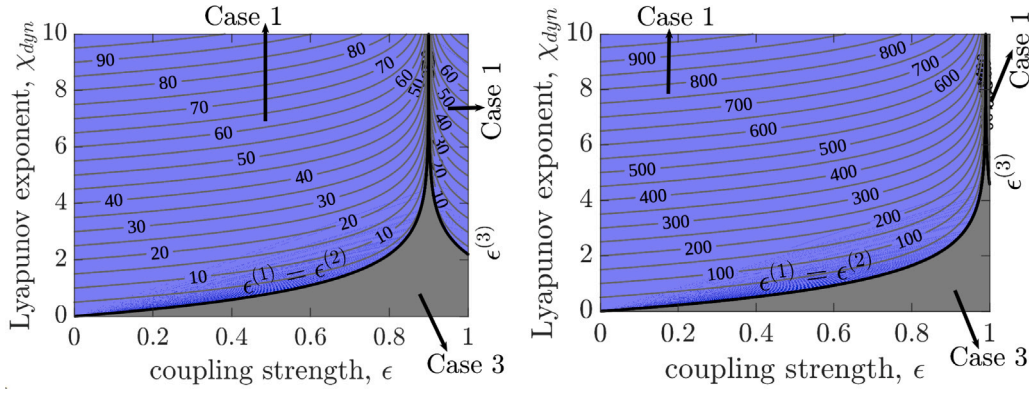
**Fig. 5.** Regions with different Lyapunov spectra and entropy rates for coupled maps in complete graphs. Control parameters: coupling strength between the maps, $\epsilon$, and map's chaoticity before coupling, $\chi_{dyn}$. Left panel: 3 regions with different collective dynamics for $N = 10$ chaotic maps according to the coupled system's Lyapunov exponents (coloured areas), where boundaries are the critical coupling strengths $\epsilon^{(1)} = \epsilon^{(2)}$ and $\epsilon^{(3)}$ [Eq. (19)]. Contour lines show constant-valued entropy rates, $h$. Right panel: same results but for $N = 100$ maps.

This means that for finite complete graphs, the system can only be in Case 1 (i.e., incoherent chaos), Case 3 (i.e., chaotic synchronisation), or Case 2 - Type II (i.e., chaos due to folded modes).

*Extensivity in complete graphs.* For the Case 1 region when all positive LEs come from unfolded modes ($n > 0$), we get

$$h_1 = N \chi_{dyn} + (N - 1) \log \left[1 - \epsilon \frac{N}{N - 1}\right]. \tag{20}$$

The first term is extensive because it is proportional to $N$. In the limit $N \to \infty$, $N/(N - 1) \to 1$ and the argument of the logarithm is constant and positive ($\to 1 - \epsilon$). So, the second term also is extensive, making Case 1 of complete graphs an extensive chaotic region.

For the Case 1 region when all positive LEs come from folded modes ($n > 0$), we get

$$h_1 = N \chi_{dyn} + (N - 1) \log \left[\epsilon \frac{N}{N - 1} - 1\right]. \tag{21}$$

However, this region disappears as $N \to \infty$ because the boundary $\epsilon^{(3)}_{C_N(N-1)} \to 1 + \exp(-\chi_{dyn})$, which is larger than 1 for any $\chi_{dyn} > 0$.

This means that the coupled maps in complete graphs can be either in Case 1 or Case 3 for the thermodynamic limit, where Case 3 is not extensive because $h_3 = \chi_{dyn}$ for all $N$ and control parameter values in this region.

*Examples for complete graphs.* When $\chi_{dyn} \to \infty$, then all critical couplings in Eq. (19) collapse, making $\epsilon^{(1)}_{C_N(N-1)}(\chi_{dyn} \to \infty) = \epsilon^{(2)}_{C_N(N-1)}(\chi_{dyn} \to \infty) = \epsilon^{(3)}_{C_N(N-1)}(\chi_{dyn} \to \infty) = (N - 1)/N$. This behaviour can be observed in the examples of Fig. 5, where the left [right] panel shows that these critical couplings tend to 0.9 [0.99] when $N = 10$ [$N = 100$] as $\chi_{dyn} \to \infty$.

The extensivity property of Case 1 for finite complete graphs can be observed in Fig. 6, where the specific entropy rate $\eta = h_1/N$ constant values (contour lines), with $h_1$ determined by Eq. (20), become straight vertical lines as $N$ is increased.

While the system is finite but increasing in size (as in Fig. 6), we can derive an expression for the coupling strength tuning needed to maintain a constant $\eta$ value in the Case 1 region. We impose that $h_1 \propto N$ in Eq. (20) and invert to find $\epsilon$ as a function of $N$. Namely, we set $\beta N = (N - 1) \log[1 - \epsilon N/(N - 1)]$, with $\beta = h_1 - \chi_{dyn} > 0$ a constant. Then,

$$\epsilon(N) = \frac{N - 1}{N} \left[1 - \exp\left(\beta \frac{N}{N - 1}\right)\right] \tag{22}$$

is the coupling strength that makes $\eta = \beta + \chi_{dyn} = $ constant, which are the contour lines in Fig. 6.

We can assign a value to $\beta$ in Eq. (22) based on the thermodynamic limit of the system ($N \to \infty$) or for 2 coupled maps ($N = 2$), which is the smallest complete graph. When $N \to \infty$, $\epsilon_\infty \equiv \lim_{N \to \infty} \epsilon(N) =$
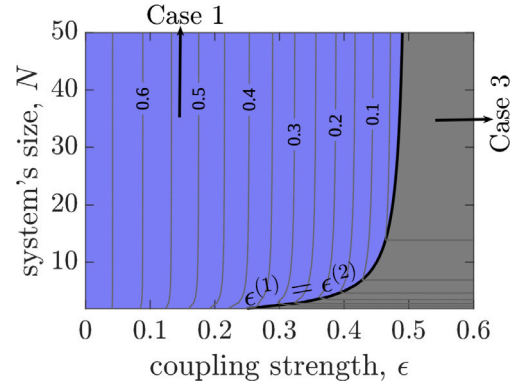


**Fig. 6.** Specific entropy rates for chaotic maps coupled in complete graphs. The chaotic maps have fixed chaoticity of $\chi_{dyn} = \log(2)$ when isolated and their coupled dynamics is controlled by $\epsilon$ and $N$ (as in Fig. 4). Shaded regions differentiate the 2 possible dynamical scenarios: incoherent chaos (blue) and chaotic synchronisation (grey). The critical coupling strength $\epsilon^{(2)}$ separates these cases [Eq. (19)]. Contour lines show constant values for the specific entropy rate $\eta = h/N$ [Eq. (20) for $h_1/N$ and $h_3/N = \chi_{dyn}/N$].

$1 - \exp(\beta)$, which implies that $\beta = \log[1 - \epsilon_\infty]$. This means that we can rewrite Eq. (22) as

$$\epsilon(N) = \frac{N - 1}{N} \left[1 - (1 - \epsilon_\infty)^{\frac{N}{N-1}}\right].$$

Similarly, when $N = 2$, we have that $\epsilon_2 \equiv \epsilon(N = 2) = \frac{1}{2}[1 - \exp(2\beta)]$, which implies that $\beta = \frac{1}{2} \log[1 - 2\epsilon_2]$. This means that we can rewrite Eq. (22) as

$$\epsilon(N) = \frac{N - 1}{N} \left[1 - (1 - 2\epsilon_2)^{\frac{N}{2(N-1)}}\right].$$

## 4. Discussion

Our results show that the Lyapunov exponents (LE) of $N$ identical, one-dimensional, chaotic maps with constant derivative, coupled diffusively in regular graphs [31] can be classified into 5 disjoint cases (see Fig. 1). These cases appear in different regions of the control parameters' space, which is defined by the isolated map's chaoticity, $\chi_{dyn}$, and coupling strength, $\epsilon$ (see Fig. 2). We find closed-form expressions for the bounds of these regions, finding the critical values of $\epsilon$ as a function of the graph's spectral properties and $\chi_{dyn}$ [see Eqs. (7), (8), and (9)]. These results show that there is one case (Case 2 - Type II) that can only appear if the regular graph is such that $\lambda_F + \lambda_M > 2k$, e.g., in a ring graph (see Figs. 2 and 3).

We find that the number of different collective dynamics emerging in the parameter space depends on whether the regular graph has $\lambda_F + \lambda_M > 2k$ (with 5 possible LE cases) or $\lambda_F + \lambda_M < 2k$ (with 4 possible cases) – Fig. 2. We note that this spectral distinction for regular graphs also arises when analysing the stability of the synchronisation manifold – as detailed in our previous work [22] – and is related to different classes of synchronisation [36].

For the analysis of Ruelle's conjecture [8], we find closed-form expressions for the LEs ($\chi_n$) and entropy rates ($h$) of rings [see Eqs. (11), (13), (15), and (17)] and complete graphs [see Eqs. (18), (20) and (21)]. These results are illustrated in Figs. 4 and 6, which show that these two types of coupled map graphs are extensive. In particular, the ring coupled system is extensive for any coupling $0 < \epsilon < 1$ outside the chaotic synchronisation region, which has $N - 1$ negative LE and is vanishingly small (see Fig. 4). Similarly, the complete graph is extensive outside the chaotic synchronisation region, which implies any coupling $0 < \epsilon < \epsilon^{(1)} = [1 - \exp(-\chi_{dyn})](N-1)/N$ (see Fig. 6).

We note that our results on the extensivity of coupled maps in ring and complete graphs align with previous works [8,37] (particularly for the ring graph, which is expected because of the local type of coupling). We also note that rings and complete graphs have been used as the building blocks of multiplex networks [19,20], where we get some differences with these previous works which divide the LE spectrum into two classes. For example, we find that the extensivity of coupled maps in ring graphs is valid for any $\epsilon \in (0, 1]$, contrary to the necessary upper bound derived in Refs. [19] when analysing a single layer of the multiplex network. Similarly, our $\epsilon^{(1)}$ upper bound [Eq. (19)] for the extensivity of coupled maps in complete graphs is less restrictive than that of Refs. [19,20]. We believe that these differences with our work arise because those works make derivations in the finite-limit size (i.e., $h \propto N$), instead of analysing $h$ in the thermodynamic limit (i.e., $N \to \infty$). When restricting our analysis to the finite-limit size, then our results match those from Refs. [19,20].

Although our work is restricted by the type graphs chosen, it can help to find approximate expressions in some closely regular random graphs, such as the Watts–Strogatz small-world network model [38]. Similarly, our work can be used to find the Lyapunov dimension of the emerging attractors by means of the Kaplan-York conjecture [21].

## 5. Conclusion

In this work, we introduce a classification for the Lyapunov exponent's (LE) spectrum of $N$ identical, one-dimensional, chaotic maps with constant derivative, that we couple diffusively in different regular graphs [31]. We introduce this classification in order to: differentiate the collective dynamics emerging when using different parameters, obtain closed-form expressions for critical parameters and entropy rates for each collective dynamic, and study the system's extensivity properties.

Our classification is based on the sign of the LEs and their relationship to the graph's Laplacian eigenvalue modes, resulting in 5 cases which represent 5 different collective behaviours. We obtain the LE's spectrum by making a linear approximation of the coupled system around a generic orbit, which decouples the map's dynamics from the graph's topology — similarly to the approach followed in the Master Stability Function [39]. Because the maps have constant derivative (i.e., we have an $N$-dimensional system with a constant Jacobian), the resultant LEs are valid for the entire phase space — not as the LEs obtained when using the MSF, which are conditioned to the synchronisation manifold. Our results are valid for any generic regular graph or map – as long as the maps have constant positive derivative and are identical – complementing other studies that focus on synchronisation properties [22,36] and aligning with previous work on extensive chaos [8,19,20,37].

Aside the introduction of our LE classification, we also provide the boundaries in parameter space for the different cases and subtypes proposed, as well as analysing their properties for finite and infinite graphs. We also show that our classification allows to capture differences in the complexity of the underlying attractors of the coupled system through the entropy rate, but also how it changes when the coupling strength or the Lyapunov exponent of the isolated map is modified. In this sense, we show the practical use of our classification, by analysing the extensive properties of coupled maps in ring and in complete graphs from their entropy rates. Moreover, our derivations can be used in other calculations that require LEs, such as finding the fractal dimensions of the emerging chaotic attractors [21].

## Declaration of competing interest

The authors declare that they have no known competing financial interests or personal relationships that could have appeared to influence the work reported in this paper.

## Data availability

No data was used for the research described in the article.

## Acknowledgements

## Appendix

*A.1. Closed sums derivations*

Here we show the derivation of the first terms of the Maclaurin expansion for

$$\sum_{n=1}^{N-1} \sum_{j=1}^{\infty} \left[ 2\epsilon \sin^2 \left( \frac{\pi n}{N} \right) \right]^j \frac{1}{j}. \tag{23}$$

For $j = 1$, the term from Eq. (23) is

$$\sum_{n=1}^{N-1} 2\epsilon \sin^2 \left( \frac{\pi n}{N} \right) = \sum_{n=1}^{N-1} \epsilon \left( 1 - \cos \left( \frac{2\pi n}{N} \right) \right),$$

where the right-hand side (*r.h.s.*) expression is obtained by applying the power-reduction identity, i.e., $2\sin^2(x) = 1 - \cos(2x)$. Summing the first term, and writing the sine in its exponential form, we obtain,

$$r.h.s. = \sum_{n=1}^{N-1} \epsilon \left( 1 - \cos \left( \frac{2\pi n}{N} \right) \right) = \epsilon \left( N - 1 - \sum_{n=1}^{N-1} \left[ \exp \left( i \frac{2\pi n}{N} \right) + \exp \left( -i \frac{2\pi n}{N} \right) \right] \frac{1}{2} \right).$$

Now we write every summation as a geometric sum, then

$$r.h.s. = \epsilon \left( N - 1 - \left[ \sum_{n=0}^{N-1} \exp \left( i \frac{2\pi n}{N} \right) + \sum_{n=0}^{N-1} \exp \left( -i \frac{2\pi n}{N} \right) - 2 \right] \frac{1}{2} \right)$$

$$= \epsilon \left( N - \left[ \sum_{n=0}^{N-1} \exp \left( i \frac{2\pi n}{N} \right) + \sum_{n=0}^{N-1} \exp \left( -i \frac{2\pi n}{N} \right) \right] \frac{1}{2} \right),$$

where these geometric sum are identically null. This is,

$$\sum_{n=0}^{N-1} \exp \left( i \frac{2\pi n}{N} \right) = \frac{1 - \exp(2\pi i)}{1 - \exp(2\pi i/N)} = 0,$$

$$\sum_{n=0}^{N-1} \exp \left( -i \frac{2\pi n}{N} \right) = \frac{1 - \exp(-2\pi i)}{1 - \exp(-2\pi i/N)} = 0,$$

since $\exp(\pm 2\pi i) = 1$. Thus $r.h.s. = \epsilon N$.

For $j = 2$, the term from Eq. (23) is

$$2\epsilon^2 \sum_{n=1}^{N-1} \sin^4\left(\frac{\pi n}{N}\right) = \frac{\epsilon^2}{4} \sum_{n=1}^{N-1} \left[3 - 4\cos\left(\frac{2\pi n}{N}\right) + \cos\left(\frac{4\pi n}{N}\right)\right],$$

where again, the $r.h.s.$ expression is obtained by applying the power-reduction identity: $8\sin^4(x) = 3 - 4\cos(2x) + \cos(4x)$. By repeating the work done for the case $j = 1$, the first sum is carried out and the cosines are written in their exponential form,

$$r.h.s. = \frac{\epsilon^2}{4}\left[3N - 3 - 2\sum_{n=1}^{N-1}\left(\exp\left(i\frac{2\pi n}{N}\right) + \exp\left(-i\frac{2\pi n}{N}\right)\right)\right.$$
$$\left. + \frac{1}{2}\sum_{n=1}^{N-1}\left(\exp\left(i\frac{4\pi n}{N}\right) + \exp\left(-i\frac{4\pi n}{N}\right)\right)\right].$$

We can rewrite again the summations as geometric sums,

$$r.h.s = \frac{\epsilon^2}{4}\left[3N - 3 - 2\sum_{n=0}^{N-1}\left(\exp\left(i\frac{2\pi n}{N}\right) + \exp\left(-i\frac{2\pi n}{N}\right)\right) + 4\right.$$
$$\left. + \frac{1}{2}\sum_{n=0}^{N-1}\left(\exp\left(i\frac{4\pi n}{N}\right) + \exp\left(-i\frac{4\pi n}{N}\right)\right) - 1\right]$$
$$= \frac{\epsilon^2}{4}\left[3N - 2\sum_{n=0}^{N-1}\exp\left(i\frac{2\pi n}{N}\right) + 2\sum_{n=0}^{N-1}\exp\left(-i\frac{2\pi n}{N}\right)\right.$$
$$\left. + \frac{1}{2}\sum_{n=0}^{N-1}\exp\left(i\frac{4\pi n}{N}\right) + \frac{1}{2}\sum_{n=0}^{N-1}\exp\left(-i\frac{4\pi n}{N}\right)\right],$$

where, by the same arguments as for case $j = 1$, every summation is identically null. Finally we obtain $r.h.s. = 3\epsilon^2/4$.

For $j = 3$, similar work is performed. Here, the term from Eq. (23) is

$$\frac{8}{3}\epsilon^3 \sum_{n=1}^{N-1}\sin^6\left(\frac{\pi n}{N}\right) = \frac{\epsilon^3}{12}\sum_{n=1}^{N-1}\left[10 - 15\cos\left(\frac{2\pi n}{N}\right) + 6\cos\left(\frac{4\pi n}{N}\right) - \cos\left(\frac{6\pi n}{N}\right)\right],$$

where the $r.h.s.$ expression corresponds to a power-reduction identity, i.e., $32\sin^6(x) = 10 - 15\cos(2x) + 6\cos(4x) - \cos(6)$. Once again, we get

$$r.h.s. = \frac{\epsilon^3}{12}\left[10N - 10 + \sum_{n=1}^{N-1}\left(-\frac{15}{2}\left(\exp\left(i\frac{2\pi n}{N}\right) + \exp\left(-i\frac{2\pi n}{N}\right)\right)\right.\right.$$
$$\left.\left. + 3\left(\exp\left(i\frac{4\pi n}{N}\right) + \exp\left(-i\frac{4\pi n}{N}\right)\right) - \frac{1}{2}\left(\exp\left(i\frac{2\pi n}{N}\right) + \exp\left(-i\frac{2\pi n}{N}\right)\right)\right)\right]$$
$$= \frac{\epsilon^3}{12}\left[10N + \sum_{n=0}^{N-1}\left(-\frac{15}{2}\left(\exp\left(i\frac{2\pi n}{N}\right) + \exp\left(-i\frac{2\pi n}{N}\right)\right)\right.\right.$$
$$\left.\left. + 3\left(\exp\left(i\frac{4\pi n}{N}\right) + \exp\left(-i\frac{4\pi n}{N}\right)\right) - \frac{1}{2}\left(\exp\left(i\frac{2\pi n}{N}\right) + \exp\left(-i\frac{2\pi n}{N}\right)\right)\right)\right]$$
$$= \epsilon^3\left[\frac{5}{6}N + \frac{1}{12}\sum_{n=0}^{N-1}\left(-\frac{15}{2}\left(\exp\left(i\frac{2\pi n}{N}\right) + \exp\left(-i\frac{2\pi n}{N}\right)\right)\right.\right.$$
$$\left.\left. + 3\left(\exp\left(i\frac{4\pi n}{N}\right) + \exp\left(-i\frac{4\pi n}{N}\right)\right) - \frac{1}{2}\left(\exp\left(i\frac{2\pi n}{N}\right) + \exp\left(-i\frac{2\pi n}{N}\right)\right)\right)\right],$$

where every sum is identically null. So, $r.h.s. = 5\epsilon^3 N/6$.

# References

[1] Holland JH. Complexity: A very short introduction. OUP Oxford; 2014.
[2] Mitchell M. Complexity: A guided tour. Oxford University Press; 2009.
[3] Mitchell M, Newman M. Complex systems theory and evolution. Encycl Evol 2002;1:1–5.
[4] Dunning-Davies J. On the meaning of extensivity. Phys Lett A 1983;94(8):346–8.
[5] Touchette H. When is a quantity additive, and when is it extensive? Physica A 2002;305(1–2):84–8.
[6] Tsallis C, Gell-Mann M, Sato Y. Extensivity and entropy production. Europhys News 2005;36(6):186–9.
[7] Tsallis C. Nonadditive entropy: The concept and its use. Eur Phys J A 2009;40(3):257–66.
[8] Ruelle D. Large volume limit of the distribution of characteristic exponents in turbulence. Comm Math Phys 1982;87(2):287–302.
[9] Livi R, Politi A, Ruffo S. Distribution of characteristic exponents in the thermodynamic limit. J Phys A: Math Gen 1986;19(11):2033.
[10] Pesin YB. Characteristic Lyapunov exponents and smooth ergodic theory. Russian Math Surveys 1977;32(4):55.
[11] Latora V, Baranger M. Kolmogorov–Sinai entropy rate versus physical entropy. Phys Rev Lett 1999;82(3):520.
[12] Egolf DA, Greenside HS. Relation between fractal dimension and spatial correlation length for extensive chaos. Nature 1994;369(6476):129–31.
[13] Egolf DA, Melnikov IV, Pesch W, Ecke RE. Mechanisms of extensive spatiotemporal chaos in Rayleigh-Bénard convection. Nature 2000;404(6779):733–6.
[14] Paul MR, Einarsson MI, Fischer PF, Cross MC. Extensive chaos in Rayleigh-Bénard convection. Phys Rev E 2007;75(4):045203.
[15] Karimi A, Paul MR. Extensive chaos in the Lorenz–96 model. Chaos 2010;20(4):043105.
[16] Luccioli S, Olmi S, Politi A, Torcini A. Collective dynamics in sparse networks. Phys Rev Lett 2012;109(13):138103.
[17] Ku WL, Girvan M, Ott E. Dynamical transitions in large systems of mean field–coupled Landau–Stuart oscillators: Extensive chaos and cluster states. Chaos 2015;25(12):123122.
[18] Monteforte M, Wolf F. Dynamical entropy production in spiking neuron networks in the balanced state. Phys Rev Lett 2010;105(26):268104.
[19] Antonopoulos CG, Baptista MS. Maintaining extensivity in evolutionary multiplex networks. PLoS One 2017;12(4):e0175389.
[20] Araujo MA, Baptista MS. Extensivity in infinitely large multiplex networks. Appl Netw Sci 2019;4(1):1–18.
[21] Frederickson P, Kaplan JL, Yorke ED, Yorke JA. The Liapunov dimension of strange attractors. J Differential Equations 1983;49(2):185–207.
[22] Gancio J, Rubido N. Critical parameters of the synchronisation's stability for coupled maps in regular graphs. Chaos Solitons Fractals 2022;158:112001.
[23] Löwdin PO, Pauncz R, De Heer J. On the calculation of the inverse of the overlap matrix in cyclic systems. J Math Phys 1960;1(6):461–7.
[24] Kalman D, White JE. Polynomial equations and circulant matrices. Amer Math Monthly 2001;108(9):821–40.
[25] Zhang H, Yang Y. Resistance distance and Kirchhoff index in circulant graphs. Int J Quantum Chem 2007;107(2):330–9.
[26] Gershgorin SA. Uber die abgrenzung der eigenwerte einer matrix. Izv. Akad. Nauk SSSR Ser. Mat. 1931;(6):749–54.
[27] Chung FR, Graham FC. Spectral graph theory, no. 92. American Mathematical Society; 1997.
[28] McKay BD. The expected eigenvalue distribution of a large regular graph. Linear Algebra Appl 1981;40:203–16.
[29] Jakobson D, Miller SD, Rivin I, Rudnick Z. Eigenvalue spacings for regular graphs. In: Emerging applications of number theory. New York, NY: Springer; 1999, p. 317–27.
[30] Dumitriu I, Pal S. Sparse regular random graphs: spectral density and eigenvectors. Ann Probab 2012;40(5):2197–235.
[31] Kaneko K. Period-doubling of kink-antikink patterns, quasiperiodicity in antiferro-like structures and spatial intermittency in coupled logistic lattice: Towards a prelude of a field theory of chaos. Progr Theoret Phys 1984;72(3):480–6.
[32] Oseledets VI. A multiplicative ergodic theorem. Lyapunov characteristic numbers for dynamical systems. Trans. Moscow Math. Soc. 1968;19:197–231, Moscov.Mat.Obsch.19 (1968) 179-210.
[33] Xie F, Cerdeira HA. Coherent-ordered transition in chaotic globally coupled maps. Phys Rev E 1996;54(4):3235.
[34] Anteneodo C, Pinto SEDS, Batista AM, Viana RL. Analytical results for coupled-map lattices with long-range interactions. Phys Rev E 2003;68(4):045202.
[35] Jost J, Joy MP. Spectral properties and synchronization in coupled map lattices. Phys Rev E 2001;65(1):016201.
[36] Boccaletti S, Latora V, Moreno Y, Chavez M, Hwang DU. Complex networks: Structure and dynamics. Phys Rep 2006;424(4–5):175–308.
[37] Takeuchi KA, Chaté H, Ginelli F, Politi A, Torcini A. Extensive and subextensive chaos in globally coupled dynamical systems. Phys Rev Lett 2011;107(12):124101.
[38] Watts DJ, Strogatz SH. Collective dynamics of 'small-world' networks. Nature 1998;393(6684):440–2.
[39] Pecora LM, Carroll TL. Master stability functions for synchronized coupled systems. Phys Rev Lett 1998;80(10):2109.